

Experimental implementation of a continuous-time quantum random walk on a solid-state quantum information processor

Maimaitiyiming Tusun(麦麦提依明·吐孙)[1,2,3,4], Yang Wu(伍旸)[1,2,3], Wenquan Liu(刘文权)[1,2,3], Xing Rong(荣星)[1,2,3], Jiangfeng Du(杜江峰)[1,2,3]

Citation: Chin. Phys. B . 2019, 28(11): 110302 . **doi:** 10.1088/1674-1056/ab44ae
Journal homepage: http://cpb.iphy.ac.cn; http://iopscience.iop.org/cpb

What follows is a list of articles you may be interested in

Tunable coupling between Xmon qubit and coplanar waveguide resonator

He-Kang Li(李贺康), Ke-Min Li(李科敏), Hang Dong(董航), Qiu-Jiang Guo(郭秋江), Wu-Xin Liu(刘武新), Zhan Wang(王战), Hao-Hua Wang(王浩华), Dong-Ning Zheng(郑东宁)

Chin. Phys. B . 2019, 28(8): 080305 . **doi:** 10.1088/1674-1056/28/8/080305

Realization of *t*-bit semiclassical quantum Fourier transform on IBM's quantum cloud computer

Xiang-Qun Fu(付向群), Wan-Su Bao(鲍皖苏), He-Liang Huang(黄合良), Tan Li(李坦), Jian-Hong Shi(史建红), Xiang Wang(汪翔), Shuo Zhang(张硕), Feng-Guang Li(李风光)

Chin. Phys. B . 2019, 28(2): 020302 . **doi:** 10.1088/1674-1056/28/2/020302

Coherent attacks on a practical quantum oblivious transfer protocol

Guang-Ping He(何广平)

Chin. Phys. B . 2018, 27(10): 100308 . **doi:** 10.1088/1674-1056/27/10/100308

Demonstration of quantum permutation parity determine algorithm in a superconducting qutrit

Kunzhe Dai(戴坤哲), Peng Zhao(赵鹏), Mengmeng Li(李蒙蒙), Xinsheng Tan(谭新生), Haifeng Yu(于海峰), Yang Yu(于扬)

Chin. Phys. B . 2018, 27(6): 060305 . **doi:** 10.1088/1674-1056/27/6/060305

Realization of quantum Fourier transform over Z_N

Fu Xiang-Qun, Bao Wan-Su, Li Fa-Da, Zhang Yu-Chao

Chin. Phys. B . 2014, 23(2): 020306 . **doi:** 10.1088/1674-1056/23/2/020306

Experimental implementation of a continuous-time quantum random walk on a solid-state quantum information processor*

Maimaitiyiming Tusun(麦麦提依明·吐孙)[1,2,3,4], Yang Wu(伍旸)[1,2,3], Wenquan Liu(刘文权)[1,2,3], Xing Rong(荣星)[1,2,3,†], and Jiangfeng Du(杜江峰)[1,2,3,‡]

[1] *Hefei National Laboratory for Physical Sciences at the Microscale, and Department of Modern Physics, University of Science and Technology of China, Hefei* 230026, *China*

[2] *CAS Key Laboratory of Microscale Magnetic Resonance, University of Science and Technology of China, Hefei* 230026, *China*

[3] *Synergetic Innovation Center of Quantum Information and Quantum Physics, University of Science and Technology of China, Hefei* 230026, *China*

[4] *School of Physics and Electronic Engineering, Xinjiang Normal University, Urumqi* 830054, *China*

(Received 8 July 2019; revised manuscript received 27 August 2019; published online 30 October 2019)

There are some problems that quantum computers seem to be exponentially faster than classical computers, like factoring large numbers, machine learning, and simulation of quantum systems. Constructing an appropriate quantum algorithm becomes more important for solving these specific problems. In principle, any quantum algorithm can recast by a quantum random walk algorithm. Although quantum random walk with a few qubits has been implemented in a variety of systems, the experimental demonstration of solid-state quantum random walk remains elusive. Here we report the experimental implementation of the quantum continuous-time random walk algorithm by a two-qubit quantum processor in a nitrogen–vacancy center in diamond. We found that quantum random walk on a circle does not converge to any stationary distribution and exhibit a reversible property. Our results represent a further investigation of quantum walking dynamics in solid spin platforms, may also lead to other practical applications by the use of quantum continuous-time random walk for quantum algorithm design and quantum coherence transport.

Keywords: quantum computations, quantum algorithm, color centers

PACS: 03.67.Lx, 07.05.Kf, 61.72.Ji **DOI:** 10.1088/1674-1056/ab44ae

1. Introduction

Richard Feynman[1] proposed the idea of quantum computing for the first time in 1982. He believes that computers built according to the principles of quantum mechanics are more efficient than classical computers in dealing with a certain type of problem. Only at the end of the 20th century, Deutsch[2] and Shor[3] discovered the first two famous quantum algorithms and since then the research of quantum computing has been developed more rapidly. Creating an efficient quantum algorithm plays a crucial role in the manufacture of the quantum computer. Unfortunately, finding a new quantum algorithm is a challenging task.

Quantum random walk (QRW) is a fundamental model of dynamical process and has extensive application in science, such as fast hitting tasks[4] and energy transport simulation.[5] In the quantum regime, quantum state has the characteristics of quantum superposition and quantum coherence. Therefore, QRW shows different behaviors from its classic version.[6,7] These characteristics allow QRW to simulate large-scale quantum many-body systems and realize universal quantum computation without time-dependent control.[8] For instance, some theoretical researchers have been revealed that QRWs propagating in one dimension (1D) have better transmission characteristics than 1D classical random walks.[9] A dozen years ago, a quantum search algorithm, which is based on the framework of QRW algorithm with remarkable speed up to their corresponding classical algorithm, was reported in Ref. [10]. Some researchers showed that in principle, any quantum algorithm can be recast as a quantum walk algorithm.[11] QRWs have been successfully implemented in systems as diverse as NMR,[12,13] bulk,[14] and fibre[15] optics, trapped ions,[16,17] trapped neutral atoms,[18] superconducting qubits,[8] and photonics.[19–22]

Here, we report an experimental realization of the quantum continuous-time random walk (CTRW) algorithm in the nitrogen-vacancy (NV) center in diamond by a two-qubit programmable quantum processor. We found that QRW has completely different probability distributions from classical random walk. While the probability distributions of the classic CTRW exhibit a uniform distribution, the probability distributions of the quantum CTRW show an oscillating trend.

The concept of quantum CTRW was proposed in

*Project supported by the National Key Research and Development Program of China (Grant Nos. 2018YFA0306600 and 2016YFB0501603), the National Natural Science Foundation of China (Grant No. 11761131011), the Fund from the Chinese Academy of Sciences (Grant Nos. GJJSTD20170001, QYZDY-SSW-SLH004, and QYZDB-SSW-SLH005), the Anhui Initiative Fund in Quantum Information Technologies, China (Grant No. AHY050000), and the Youth Innovation Promotion Association of the Chinese Academy of Sciences.

†Corresponding author. E-mail: xrong@ustc.edu.cn

‡Corresponding author. E-mail: djf@ustc.edu.cn

© 2019 Chinese Physical Society and IOP Publishing Ltd

Ref. [23]. For the CTRW on an undirected circle, four nodes can be grouped in columns indexed by $\{0,1,2,3\}$ as shown in Fig. 1(a). Each node is connected with the line on the circle. Every step only occurs between two adjacent nodes. The jumping rate from a node to its neighbour is given by γ, which is a fixed, time-independent constant. This means that the movement between adjacent nodes is determined by the probability γ per unit time. The corresponding 4×4 generator matrix[23] is defined by

$$H=\begin{pmatrix} 2\gamma & -\gamma & 0 & -\gamma \\ -\gamma & 2\gamma & -\gamma & 0 \\ 0 & -\gamma & 2\gamma & -\gamma \\ -\gamma & 0 & -\gamma & 2\gamma \end{pmatrix}. \tag{1}$$

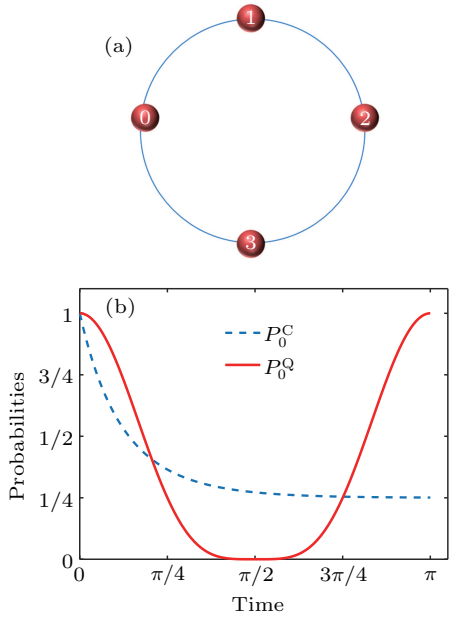


Fig. 1. Schematic diagram of a four-node random walk and corresponding two different types of probabilities of time evolution. (a) The circle with four nodes. (b) The probabilities of a particle being at the node 0 over time t in the classical and quantum version of CTRW. The blue dashed line corresponds to the classical case, and red line corresponds to the quantum case.

With such a generator matrix H, it is possible to construct a classical CTRW. The evolution of the probability distribution $P_k^{\mathrm{C}}(t)$ (superscript C indicates the classical case) at node k at time t is given by

$$\frac{\mathrm{d}}{\mathrm{d}t}P_k^{\mathrm{C}}(t)=-\sum_{l=0}^{3}H_{kl}P_l^{\mathrm{C}}(t). \tag{2}$$

The quantum CTRW can be analogized to the classical CTRW by treating the generator matrix as the Hamiltonian in quantum evolution.[23] The four basis $|0\rangle,|1\rangle,|2\rangle,|3\rangle$ correspond to four nodes $\{0,1,2,3\}$. The Schrödinger equation for $|\psi(t)\rangle$ can be written as

$$\mathrm{i}\frac{\mathrm{d}}{\mathrm{d}t}\langle k|\psi(t)\rangle=-\sum_{l=0}^{3}\langle k|H|l\rangle\langle l|\psi(t)\rangle. \tag{3}$$

By measuring the state of a particle at the time t, the probability distribution of the particle at a certain node can be obtained. The probability of the particle at node k is $P_k^{\mathrm{Q}}(t)=|\langle k|\psi(t)\rangle|^2$ (superscript Q indicates the quantum case). The conservation of probability is guaranteed by the normalization. Considering the walking particle starts moving from node 0, then the probabilities of the particle at node k at time t in the quantum and classical CTRW frames have different characteristics as shown in Fig. 1(b). The probability that a particle of a classical CTRW frame cannot return to the initial position (node 0) after a period of time exhibits gradually decay over time and finally reaches a uniform distribution at the infinite-time limit. While the probability of the particle returning to node 0 under the quantum CTRW frame exhibits periodicity.

2. Materials and methods

To implement quantum CTRW on a circle, an NV center in diamond was used in our experiment. The NV center is a defect in diamond as depicted in Fig. 2(a). The electron spin in NV center can be polarized and read out optically. The coherence time is very long even at the room temperature. The ground state of the electron spin is a spin triplet ($S=1$) splitting into three spin sublevels $|m_S=0\rangle$ and $|m_S=\pm1\rangle$. In our experiment, the two-qubit system comprises the electron spin qubit and ^{14}N nuclear spin qubit. Electron (nuclear) spin states $|m_S=0\rangle$ and $|m_S=-1\rangle$ ($|m_I=+1\rangle$ and $|m_I=0\rangle$) are encoded as the electron (nuclear) spin qubit without considering the other spin levels as shown in Fig. 2(b).

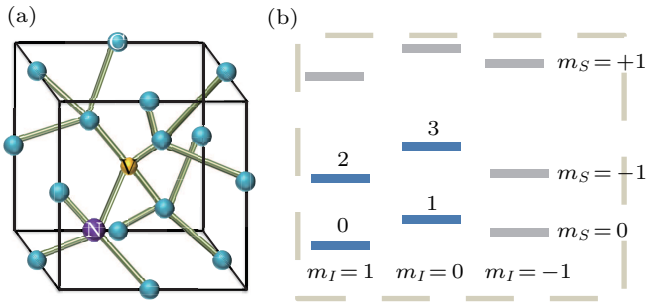


Fig. 2. Schematics of NV center in diamond. (a) Atomic structure. (b) Energy levels. The experiments were implemented on the two-qubit system which is composed of four energy levels marked by blue color. The four levels, $|m_S=0,m_I=+1\rangle$, $|m_S=0,m_I=0\rangle$, $|m_S=-1,m_I=+1\rangle$, and $|m_S=-1,m_I=0\rangle$, are denoted by $|0\rangle$, $|1\rangle$, $|2\rangle$, and $|3\rangle$.

Our diamond sample is a [100] facial bulk diamond and was mounted on a typical optically detected magnetic resonance confocal setup. The substitutional nitrogen concentration of sample is less than 5 ppb and the natural abundance of ^{13}C is about 1.1%. By applying a 532-nm green laser and a 500-Gs (1 Gs = 10^{-4} T) static magnetic field aligned parallel to the symmetry axis of the NV center, the spin state of the NV center is effectively polarized to $(m_S,m_I)=(0,+1)$.[24] The static magnetic field is created by a permanent magnet. A coplanar waveguide and a coil were used for feeding the microwave (MW) and radio frequency (RF) pulses, respectively.

Table 1. The parameters of two-qubit programmable processor for quantum CTRW algorithm.

t	α	β	δ	θ_A	φ_A	$\theta_{z,A}$	θ_B	φ_B	$\theta_{z,B}$	θ_C	φ_C	$\theta_{z,C}$	θ_D	φ_D	$\theta_{z,D}$
$\pi/12$	0	$11\pi/6$	0	$\pi/3$	π	π	$3\pi/5$	0	$3\pi/2$	$\pi/3$	π	π	$\pi/2$	$2\pi/9$	$4\pi/3$
$\pi/6$	0	0	$2\pi/3$	$\pi/2$	$-\pi/2$	$7\pi/5$	$3\pi/4$	0	π	$\pi/2$	$-\pi$	$8\pi/5$	$2\pi/5$	$-\pi/3$	$\pi/3$
$\pi/4$	2π	$3\pi/2$	0	0	π	0	$3\pi/2$	2π	0	π	$\pi/2$	0	$3\pi/2$	0	0
$\pi/3$	0	$\pi/3$	0	π	$-\pi/9$	$\pi/5$	π	$-\pi/9$	$3\pi/4$	0	$\pi/6$	0	$\pi/2$	$-\pi/3$	$5\pi/6$
$5\pi/12$	π	$\pi/6$	0	$4\pi/15$	$-\pi$	π	0	$-8\pi/9$	$3\pi/2$	$4\pi/15$	0	2π	$\pi/2$	$-7\pi/6$	$5\pi/3$
$\pi/2$	0	0	π	$-3\pi/5$	0	$-\pi/4$	π	$\pi/4$	0	$7\pi/10$	$\pi/2$	$4\pi/3$	$11\pi/12$	$11\pi/12$	$3\pi/5$
$7\pi/12$	0	0	$6\pi/5$	$\pi/2$	$-\pi/2$	$7\pi/5$	$3\pi/2$	π	0	$\pi/2$	$-\pi/10$	$7\pi/12$	$7\pi/12$	$-5\pi/6$	$5\pi/6$
$2\pi/3$	0	0	$\pi/3$	$\pi/2$	$\pi/2$	$\pi/6$	$\pi/3$	$-\pi$	π	$\pi/2$	$2\pi/3$	$6\pi/5$	$\pi/2$	$-2\pi/3$	$2\pi/3$
$3\pi/4$	0	0	$3\pi/2$	$-\pi/2$	0	$-5\pi/6$	$\pi/2$	$3\pi/2$	$\pi/2$	$3\pi/2$	$\pi/2$	$7\pi/10$	π	$13\pi/10$	$3\pi/2$
$5\pi/6$	0	$3\pi/2$	0	$2\pi/5$	π	0	$5\pi/6$	$-\pi$	$3\pi/2$	$3\pi/5$	π	0	$\pi/2$	$7\pi/6$	$\pi/3$
$11\pi/12$	0	0	$\pi/6$	$\pi/2$	$-\pi/2$	$9\pi/7$	$\pi/4$	0	π	$\pi/2$	$-\pi/5$	$7\pi/10$	$2\pi/5$	$-5\pi/6$	$5\pi/6$
π	0	2π	2π	$-11\pi/10$	$-2\pi/5$	$-\pi/3$	π	$\pi/4$	$\pi/2$	$\pi/4$	0	$7\pi/4$	$7\pi/5$	$\pi/4$	$4\pi/7$

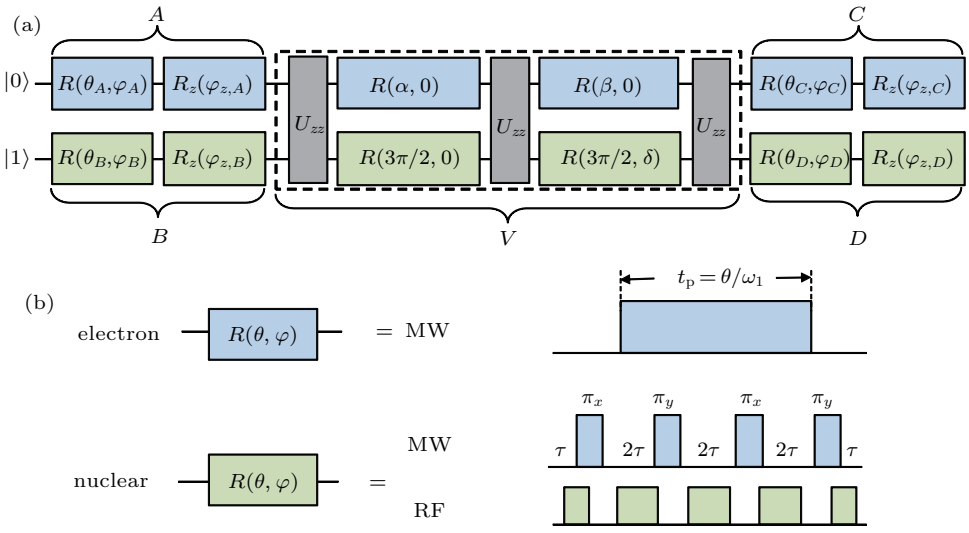


Fig. 3. Two-qubit programmable quantum processor in NV center. (a) Circuit diagrams for arbitrary unitary transformations on two qubits. The brackets highlight the decomposition of the two-qubit operation into $(C\otimes D)\cdot V\cdot(A\otimes B)$. (b) Realization of the single-qubit gates.

In our experiment, a two-qubit programmable quantum processor[25] was used to realize the time evolution of the quantum CTRW. The arbitrary two-qubit unitary operation can be implemented by the programmable quantum processor using the universal quantum circuit with altering the parameters. We chose the universal gate library consisting of single-qubit gates parameterized by the decomposition $R_z(\varphi_z)\cdot R(\theta,\varphi)$ and an entangling two-qubit gate $U_{zz}=\exp(\mathrm{i}\pi S_z\otimes I_z)$. Here $R(\theta,\varphi)=\exp[-\mathrm{i}\theta(\cos\varphi\, S_x+\sin\varphi\, S_y)]$ corresponds to a rotation of angle θ around the axis in the XY plane. Parameter φ denotes the angle between the axis of rotation and the X axis. $R_z(\varphi_z)$ represents a rotation of angle φ_z around the Z axis. S_j $(j=x,y,z)$ and I_z are the electron and nuclear spin operators, respectively. According to Eq. (3), the time evolution of the CTRW is obtained by $|\psi(t)\rangle=U(t)|\psi(0)\rangle$, where $U(t)=\exp(-\mathrm{i}Ht)$. The various $U(t)$ at different time t can be decomposed into $U(t)=(C\otimes D)\cdot V\cdot(A\otimes B)$ as shown in Fig. 3(a). The decomposition of the unitary operation U is performed following the two steps in Ref. [25]. The first step is to match the matrix eigenvalues of V in the same local equivalence class as U for confirming the three parameters α, β, and δ shown in the dashed rectangle in Fig. 3(a). The second step is to manipulate the real and orthogonal matrix eigenvectors to obtain the four remaining single qubit operations which are required to map between V and $U(t)$. According to the above two steps, quantum CTRW state evolution can be realized by the universal quantum circuit with fifteen parameters, which are α, β, δ, θ_A, φ_A, $\varphi_{z,A}$, θ_B, φ_B, $\varphi_{z,B}$, θ_C, φ_C, $\varphi_{z,C}$, θ_D, φ_D, and $\varphi_{z,D}$ as shown in Table 1.

In the experiment, the single qubit rotations on the electron spin are implemented by a hard microwave pulse as shown in Fig. 3(b). The time τ corresponds to the interaction between electron spin and nuclear spin, and t_p is pulse duration time which is controlled by the angle of rotation θ. The single qubit rotations on the nuclear spin are implemented by the decoherence-protected gates which are comprised of dynamical decoupling on the electron spin and nuclear spin driving.

3. Results and discussion

The probabilities as a function of time t are shown in Fig. 4(a), where the blue dashed curve and the gray curve are

the simulated results of the classical and quantum cases and the solid circles with error bars are the experimental results. The simulated result is achieved by considering the effect of decoherence, which is aroused by the static fluctuation of the magnetic field. Our results show that the probability of classical CTRW monotonically decreases with time and exhibits a trend of uniform distribution in the end. While the probability of quantum CTRW has a periodic behavior. The experimental results are in good agreement with the simulated ideal cases.

A straightforward method to characterize the uniformity of a distribution is to use the total variation distance between the given distribution and the uniform distribution. The classical and quantum total variation distance as a function of time t is

$$\Delta^{\mathrm{C(Q)}}(t) = \frac{1}{2}\sum_{k=0}^{3}\left|P_k^{\mathrm{C(Q)}}(t) - \frac{1}{4}\right|. \tag{4}$$

Figure 4(b) exhibits the the dependence of $\Delta^{\mathrm{C}}(t)$ and $\Delta^{\mathrm{Q}}(t)$ on time. The classical version of this CTRW approaches the uniform distribution exponentially as time lapses. In contrast, the quantum CTRW shows an oscillating behavior. An interesting property of this quantum CTRW is that $\Delta^{\mathrm{Q}}(n\pi/4\gamma) = 0$ when n is odd, which means that the probability distribution is exactly uniform at times $t = \pi/4\gamma$ and its odd multiples. While the classical CTRW only can reach the uniform distribution at the infinite-time limit. It can be seen that the experimental results are consistent with the theoretical predictions. Errors mainly come from decoherence effect and imperfect polarization. When the magnetic field strength is set to 500 Gs, the spin state of the NV center is effectively polarized to $|m_S = 0\rangle$ state. After the optical pumping, 95% of the population occupies the $|m_S = 0\rangle$ state of the electron spin and 98% of the population occupies the $|m_I = +1\rangle$ state of the nuclear spin. The imperfect polarization indicates an initialization error of about 7%.

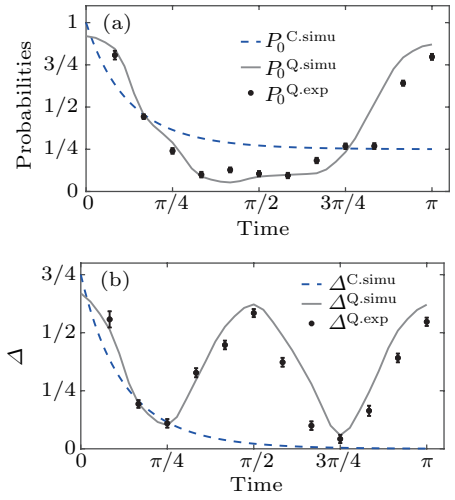


Fig. 4. Characterization of the performance of CTRWs on a circle. (a) The probabilities of the particle at node 0 at time t. (b) The total variation distances against time. The blue dashed line is the simulation results of classical CTRW. The grey lines represent simulation results of quantum CTRW considering the decoherence effect and imperfect polarization. Black dots with error bars are experimental results of the quantum CTRW. All the error bars on the data points are the standard deviations from the mean.

4. Conclusion

In conclusion, we have realized quantum CTRW algorithm with a solid-state programmable two-qubit quantum processor at room temperature. The programmable quantum processor which is based on the spin qubits in an NV center is used to implement the quantum CTRW algorithm by altering the parameters in the universal quantum circuit. The experimental results demonstrate that the quantum walk yields the oscillating behavior which is reversible and periodic, while the classical counterpart is essentially dissipative. Our work verifies the computational flexibility of the programmable processor, which paves the way to implement various algorithms in a large-scale room-temperature programmable quantum computation architecture.

References

[1] Feynman R P 1982 *Int. J. Theor. Phys.* **21** 467
[2] Deutsch D 1985 *P. Roy. Soc. Lond. Mat.* **400** 97
[3] Shor P W 1994 *Proceedings 35th Annual Symposium on Foundations of Computer Science*, November 20–22, 1994, Santa Fe, NM, USA, pp. 124–134
[4] Tang H, Franco C D, Shi Z Y, He T S, Feng Z, Gao J, Sun K, Li Z M, Jiao Z Q, Wang T Y, Kim M S and Jin X M 2018 *Nat. Photon.* **12** 754
[5] Harris N C, Steinbrecher G R, Prabhu M, Lahini Y, Mower J, Bunandar D, Chen C, Wong F N C, Baehr-Jones T, Hochberg M, Lloyd S and Englund D 2017 *Nat. Photon.* **11** 447
[6] Aharonov Y, Davidovich L and Zagury N 1993 *Phys. Rev. A* **48** 1687
[7] Childs A M, Farhi E and Gutmann S 2002 *Quantum Inf. Process.* **1** 35
[8] Yan Z, Zhang Y R, Gong M, Wu Y, Zheng Y, Li S, Wang C, Liang F, Lin J, Xu Y, Guo C, Sun L, Peng C Z, Xia K, Deng H, Rong H, You J Q, Nori F, Fan H, Zhu X and Pan J W 2019 *Science* **364** 753
[9] Mulken O and Blumen A 2006 *Phys. Rev. E* **73** 066117
[10] Shenvi N, Kempe J and Whaley K B 2003 *Phys. Rev. A* **67** 052307
[11] Childs A M 2009 *Phys. Rev. Lett.* **102** 180501
[12] Du J F, Li H, Xu X D, Shi M J, Wu J H, Zhou X Y and Han R D 2003 *Phys. Rev. A* **67** 042316
[13] Ryan C A, Laforest M, Boileau J C and Laflamme R 2005 *Phys. Rev. A* **72** 062317
[14] Do B, Stohler M L, Balasubramanian S, Elliott D S, Eash C, Fischbach E, Fischbach M A, Mills A and Zwickl B 2005 *JOSA B* **22** 499
[15] Schreiber A, Cassemiro K N, Potocek V, Gabris A, Mosley P J, Andersson E, Jex I and Silberhorn C 2010 *Phys. Rev. Lett.* **104** 050502
[16] Schmitz H, Matjeschk R, Schneider C, Glueckert J, Enderlein M, Huber T and Schaetz T 2009 *Phys. Rev. Lett. 103* 090504
[17] Zahringer F, Kirchmair G, Gerritsma R, Solano E, Blatt R and Roos C F 2010 *Phys. Rev. Lett. 104* 100503
[18] Karski M, Förster L, Choi J M, Steffen A, Alt W, Meschede D and Widera A 2009 *Science 325* 174
[19] Carolan J, Meinecke J D A, Shadbolt P J, Russell N J, Ismail N, Worhoff K, Rudolph T, Thompson M G, O Brien J L, Matthew J C F and Laing A 2014 *Nat. Photon.* **8** 621
[20] Perets H B, Lahini Y, Pozzi F, Sorel M, Morandotti R and Silberberg Y 2008 *Phys. Rev. Lett.* **100** 170506
[21] Qiang X G, Loke T, Montanaro A, Aungskunsiri K, Zhou X Q, O'Brien J L, Wang J B B and Matthews J C F 2016 *Nat. Commun.* **7** 11511
[22] Tang H, Lin X F, Feng Z, Chen J Y, Gao J, Sun K, Wang C Y, Lai P C, Xu X Y and Wang Y 2018 *Sci. Adv.* **4** eaat3174
[23] Farhi E and Gutmann S 1998 *Phys. Rev. A* **58** 915
[24] Jacques V, Neumann P, Beck J, Markham M, Twitchen D, Meijer J, Kaiser F, Balasubramanian G, Jelezko F and Wrachtrup J 2009 *Phys. Rev. Lett.* **102** 057403
[25] Wu Y, Wang Y, Qin X, Rong X and Du J F 2019 *npj Quantum Information* **5** 9
[26] Childs A M, Gosset D and Webb Z 2013 *Science* **339** 791